Thermo-acoustic Phase Modulator based on Y36-cut $LiNbO_3$ Thin Film

Xuankai Xu[1], Yushuai Liu[1,2,3], Lihui Jin[1], Peng Wu[5], Yitao Liao[5], and Tao Wu[1,2,3,4]
Email: xuxk2022@shanghaitech.edu.cn; wutao@shanghaitech.edu.cn
[1]School of Information Science and Technology, ShanghaiTech University, Shanghai, China
[2]Shanghai Institute of Microsystem and Information Technology, Chinese Academy of Sciences, Shanghai, China
[3]University of Chinese Academy of Sciences, Beijing, China
[4]Shanghai Engineering Research Center of Energy Efficient and Custom AI IC, Shanghai, China
[5]Xuzhou Liyu Advanced Technology Co. Ltd., Xuzhou, Jiangsu, China

***Abstract*—Microwave acoustic components have higher quality factors and less crosstalk than electromagnetic components. Efficient modulation of acoustic devices is essential for building large-scale multifunctional acoustic circuits. Here, we demonstrate a thermo-acoustic phase modulator based on a Y36-cut $LiNbO_3$ (LN) thin-film platform. The proposed structure integrates a 460 MHz SH_0 mode acoustic delay line and an on-chip microheater for locally changing the temperature and thus controlling the phase of the ADL. Using this approach, we achieve a phase change of more than 281° at a heating power of 20 mW, and a modulation ability of 17 °/mW in the linear modulation range, which is a 6.5 times improvement over previously reported bulk-LN platforms. Our thermo-acoustic modulators enable reconfigurable acoustic signal processing for next-generation wireless communication and microwave systems.**

Keywords—Thermo-acoustic phase modulator, SH_0 mode acoustic delay line, $LiNbO_3$ thin film Introduction

I. Introduction

Microwave acoustic devices are becoming increasingly crucial in advanced communication systems and innovative microwave signal processing research [1]-[12]. This growing interest is due to the significantly slower speed of acoustic waves compared to electromagnetic waves of the same frequency, with a speed difference of five orders of magnitude. Consequently, microwave acoustic devices feature much smaller wavelengths than their electromagnetic counterparts. These devices have successfully achieved operating frequencies in the tens of gigahertz [13], [14], making them a promising platform for advanced microwave signal processing in next-generation wireless communications. The rising demand for sophisticated communication and signal processing solutions has driven significant interest in tunable microwave acoustic devices, especially for on-chip acoustic wave modulation [15]-[19].

While electro-acoustic (EA) modulation techniques have been investigated, they generally require very high voltages to produce significant phase shifts [15], [16]. Alternatively, thermo-acoustic (TA) modulation offers a promising alternative by significantly reducing the necessary driving voltage. However, current thermo-acoustic phase modulators based on surface acoustic wave (SAW) platforms encounter challenges such as limited operational frequency, low modulation efficiency, and slow response times [17]. Suspended thin film acoustic devices have emerged as a promising solution due to their lower acoustic loss and improved electro-mechanical coupling [20]-[23]. Moreover, suspended thin film thermal devices provide excellent thermal isolation and small thermal capacity, leading to lower power consumption and faster response times [24]-[27].

This work was supported in part by the Natural Science Foundation of Shanghai (23ZR1442400), in part by Jiangsu Provincial Key Research and Development program (BE2023048), in part by the Foundation of the state key laboratory of Transducer Technology (No. SKT2303).

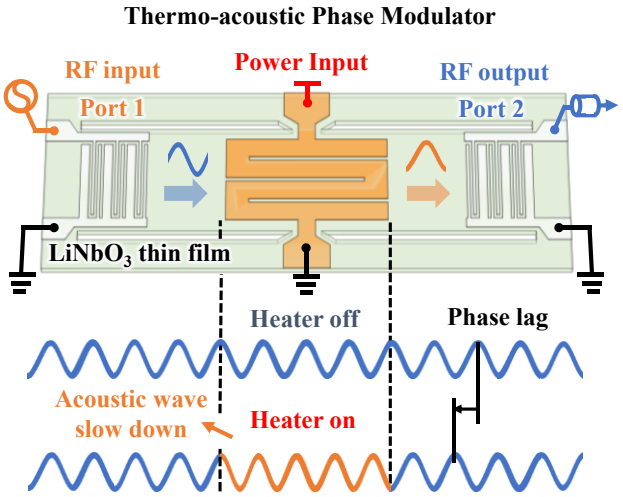

Fig. 1. Schematic of the thermo-acoustic phase modulator. The RF signal convert into acoustic wave via a single-phase unidirectional transducer (SPUDT), and modulated via a heater, when the heater is turned on, the elastic constant decreases, causing the acoustic velocity to decrease, resulting in a shorter wavelength in the modulation region, and eventually a phase lag occurs.

In this study, we present a thermo-acoustic phase modulator built on a Y36-cut $LiNbO_3$ (LN) thin-film platform. Our design incorporates a 460 MHz SH_0 mode acoustic delay line (ADL) and an on-chip microheater, enabling precise temperature control and phase adjustment of the ADL. This method achieves a phase change of over 281° at a heating power of 20 mW, with a modulation capability of 17 °/mW in the linear modulation range, marking a 6.5 times improvement over previously reported bulk-LN platforms. Our thermo-acoustic modulators offer a versatile solution for reconfigurable acoustic signal processing in next-generation wireless communication and microwave systems.

II. Design and Analysis

A. Design of thermo-acoustic phase modulator

The schematic diagram of a phase modulator utilizing Y36-cut thin-film LN is depicted in **Fig. 1**. This modulator configuration incorporates two single-phase unidirectional

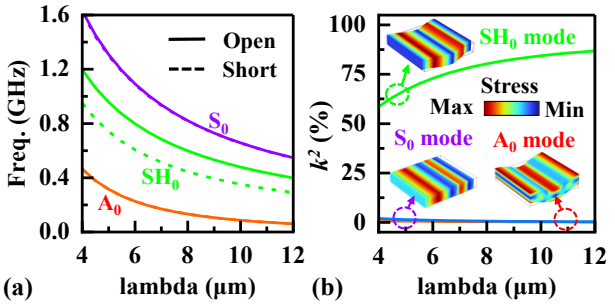

Fig. 2. FEA simulation of Y36-cut LN thin film. (a) FEA simulated dispersion curve of a 750nm Y36-cut LN thin film; (b) The calculated electromechanical coupling coefficient (k^2), the SH_0 mode possesses the highest k^2 among all the fundamental modes, which can be effectively excited.

transducers (SPUDTs) functioning as a two-port device, with a micro-heater positioned centrally. The modulation mechanism involves the activation of the micro-heater within the modulation region, which induces localized heating. This thermal perturbation leads to a reduction in the elastic constants of both the LN substrate and the aluminum (Al) micro-heater, subsequently decreasing the acoustic velocity within the device. As a result, the acoustic wavelength shortens compared to its unmodulated state, thereby inducing a phase shift following modulation.

B. Analysis of acoustic modes

Efficient acoustic wave transmission forms the basis of our phase modulator. A large piezoelectric constant enhances effective acoustic wave transmission. Y36-cut LN thin film is selected due to its substantial piezoelectric constant e_{16} along the x propagation direction. To identify the most effective acoustic mode, the dispersion curve of Y36-cut LN is simulated. **Fig. 2(a)** presents the results of finite element analysis (FEA) simulations, illustrating the dispersion characteristics of a 750 nm thick Y36-cut LN thin film. **Fig. 2(b)** provides the calculated values of the electromechanical coupling coefficient (k^2) and the mode shapes of the fundamental modes, identifying the SH_0 mode as exhibiting superior excitation efficiency among the fundamental modes.

C. Modulation simulation

To evaluate the phase modulation capability, we simulated the phase velocities of a 100 nm Al and 750 nm LN stack layer at different heating temperatures. The material properties used in the simulation are detailed in **Table I** [28]. As illustrated in **Fig. 3(a)**, the acoustic velocities decrease with increasing temperature, with an evaluation rate of 0.34 km/(s·K). The required modulation length at a heating temperature of 100 K for a 180° phase shift is depicted in **Fig. 3(b)**. Higher frequencies necessitate shorter modulation lengths due to higher phase velocities and shorter wavelengths, resulting in larger cumulative phase changes. **Fig. 3(c)** outlines the design parameters and electrical configurations of the SPUDT setup. The width of a unit cell is λ, with the width of the excited electrodes and the reflective ground being 1/8 λ and 3/8 λ, respectively. The spacing between the electrodes is 1/8 λ. **Fig. 3(d)** shows the simulated S_{21} of the acoustic delay line with an 8 μm wavelength (λ) and 10 cells (N_{cell}).

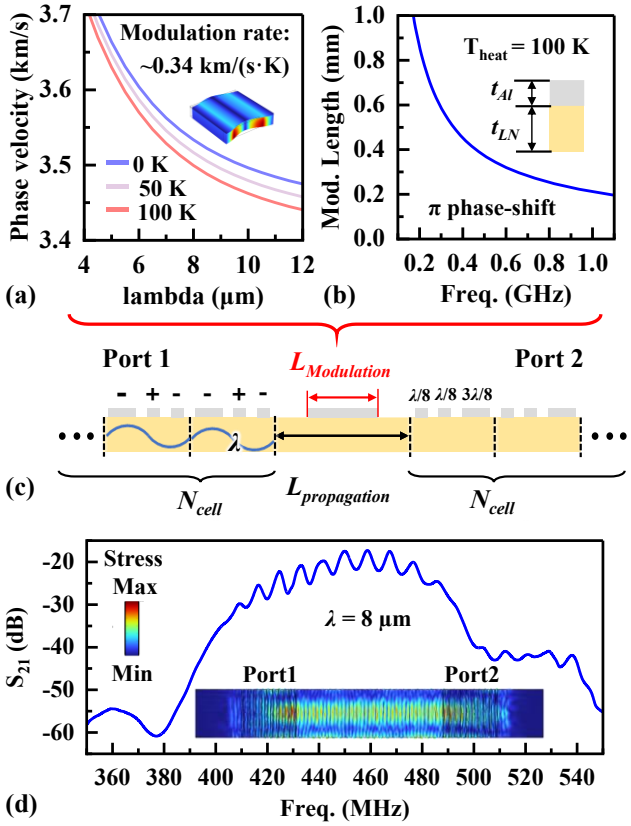

Fig. 3. Simulation analysis of thermal modulation performance and transmission performance of the SPUDT delay line. (a) Phase velocities of 100 nm Al and 750 nm LN stack layer under different heating temperatures. (b) The required modulation length at heating temperature of 100 K for 180° phase shift. (c) Schematic of the SPUDT design parameters and electric configuration. (d) The simulated performance of a SPUDT acoustic delay line with λ of 8 μm and N_{cell} of 10.

TABLE I. MATERIAL PROPERTIES USED IN SIMULATION.

Material Property		Z-Cut $LiNbO_3$ (TC, ppm/K)	Al (TC, ppm/K)
Elastic constants [GPa]	c_{11}^E	203 (-174)	E = 69 (-590)
	c_{12}^E	57.3 (-252)	
	c_{13}^E	75.2 (-159)	
	c_{14}^E	8.5 (-214)	
	c_{33}^E	242.4 (-153)	
	c_{44}^E	59.5 (-203)	
	c_{66}^E	72.8 (-143)	
Density [kg/m³]	ρ	4700	2700
Coefficient of thermal expansion [ppm/K]	α_x	(14.4)	(23.1)
	α_y	(15.9)	(23.1)
	α_z	(7.5)	(23.1)

*TC: Temperature coefficient

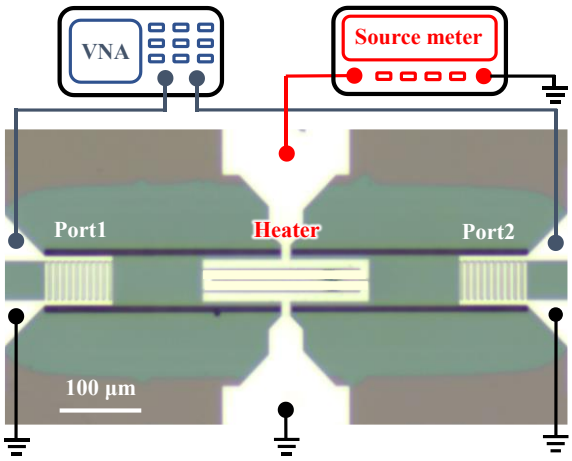

Fig. 4. The optical photo of the fabricated thermal-acoustic modulator and schematic of the testing setup. The RF transmission characteristic is measured via a vector network analyzer (VNA), the power of the heater is provided by a source meter.

III. EXPRIMENT REUST

A. Device and exprimental setup

The fabrication process started with a 750 nm Y36-cut LN on a silicon wafer. Firstly, the release boundaries of the device are defined using photoresist AZ5214, then the exposed areas were etched by ion beam etching (IBE) with a biased voltage of 300 V. Electrodes are defined in a second lithography step, and a 100 nm layer of Al is sputtered, followed by a lift-off process. Finally, the silicon underneath the device was released via XeF_2, creating a suspended LN platform. The optical image of the fabricated thermo-acoustic phase modulator and the experimental setup are illustrated in **Fig. 4**. The S-parameters of the devices were measured using a vector network analyzer (Keysight N5234B) equipped with two ports connected to ground-signal-ground (GSG) RF probes. To assess the DC bias phase control, a DC source meter (Keysight B2901A) was utilized to supply the DC voltage. In this setup, an RF signal is transformed into a shear horizontal acoustic wave by a SPUDT at Port1. This acoustic wave then propagates through the modulation area and is received by another SPUDT at Port2, where it is converted back into an RF signal for evaluating the phase change. The design parameters of the fabricated device are detailed in **Table II**. The propagation length ($L_{Propagation}$) and modulation length ($L_{Modulation}$) are designed to be 400 μm and 200 μm, respectively. The wavelength (λ) is designed to be 8 μm, targeting operation at a frequency of approximately 460 MHz. The number of cells (N_{cell}) is set to 10 to ensure effective transceiving of the acoustic wave.

TABLE II. DESIGN PARAMETERS

t_{Al} (nm)	t_{LN} (nm)	λ (μm)	N_{cell}
100	750	8	10
$L_{Propagation}$ (μm)		$L_{Modulation}$ (μm)	
400		200	

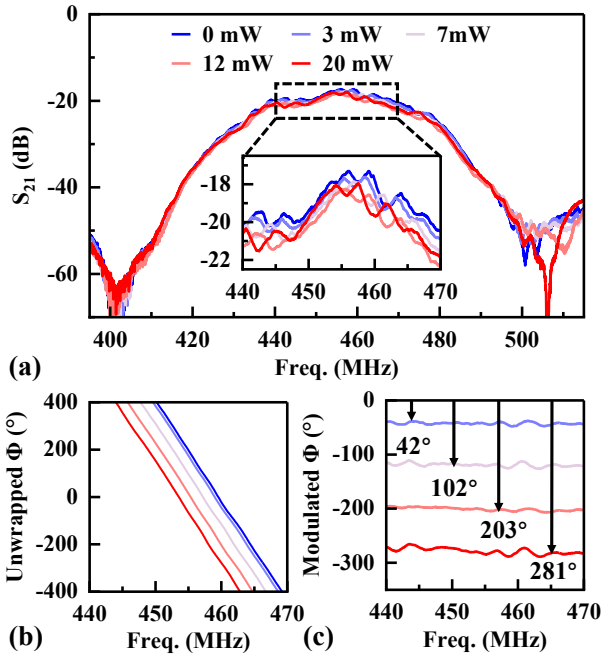

Fig. 5. (a) The measured S_{21} parameters under different input power of the heater. (b) The unwrapped phase angles. (c) The phase angle lag compared with the unmodulated phase angle.

B. DC phase modulation

The measured S_{21} parameters under different heating powers are shown in **Fig. 5(a)**. The test results demonstrate a stable frequency response despite changes in modulation power, indicating that the thermal energy is effectively localized around the modulation area and has minimal effect on the SPUDT area. **Fig. 5(b)** presents the unwrapped phase angles and the phase angle lag compared with the unmodulated phase angle, illustrating the acoustic phase shift as the modulation power increases. This shift indicates that the phase velocity of the acoustic wave decreases as the modulation temperature rises. **Fig. 5(c)** shows the modulated phases relative to the unmodulated phase across the working frequencies. The stability of the modulated phase across these frequencies is noteworthy, as it suggests that the modulator can operate consistently over a range of frequencies. Notably, at a modulation power of 20 mW, which corresponds to a heating voltage of 1 V, the modulation phase angle reaches 281°. The thin-film LN thermo-acoustic modulator demonstrates a significant modulation capability of 17 °/mW, which represents a 6.5 times improvement compared to previously reported bulk-LN platforms. The enhancement in modulation capability is attributed to the unique properties of the suspended thin-film structure. The thin-film design offers excellent thermal isolation, which minimizes the dissipation of thermal energy to surrounding areas, and a low thermal capacity, which allows for rapid and efficient temperature changes with minimal power input. These characteristics result in significantly reduced power consumption and increased modulation capability, making the thin-film LN thermo-acoustic modulator an attractive option for high-efficiency, low-power modulation applications in advanced RF and acoustic wave devices.

IV. Conclusion

In this study, we demonstrate a thermo-acoustic phase modulator based on a Y36-cut LN thin-film platform. The proposed structure integrates a 460 MHz SH_0 mode acoustic delay line and an on-chip microheater for localized temperature modulation. By leveraging the significant piezoelectric properties of Y36-cut LN and the localized heating provided by the integrated microheater, our device exhibits enhanced phase modulation capabilities. We achieve a phase change exceeding 281° at a heating power of 20 mW and a modulation ability of 17 °/mW. This performance marks a 6.5 times improvement over previously reported bulk-LN platforms. Our thermo-acoustic modulators pave the way for reconfigurable acoustic signal processing in next-generation wireless communication and microwave systems.

Acknowledgment

The authors would like to thank the ShanghaiTech Material Device Lab (SMDL) for device fabrication support.

Reference

[1] G. Giribaldi, L. Colombo, P. Simeoni, and M. Rinaldi, "Compact and wideband nanoacoustic pass-band filters for future 5G and 6G cellular radios," Nat. Commun., vol. 15, no. 1, p. 304, Jan. 2024.

[2] H. Qiao et al., "Splitting phonons: Building a platform for linear mechanical quantum computing," Science, vol. 380, no. 6649, pp. 1030–1033, Jun. 2023.

[3] Q. Zhang et al., "Gigahertz topological valley Hall effect in nanoelectromechanical phononic crystals," Nat. Electron., vol. 5, no. 3, pp. 157–163, Mar. 2022.

[4] D. D. Bühler et al., "On-chip generation and dynamic piezo-optomechanical rotation of single photons," Nat. Commun., vol. 13, no. 1, p. 6998, Nov. 2022.

[5] L. Shao et al., "Non-reciprocal transmission of microwave acoustic waves in nonlinear parity–time symmetric resonators," Nat. Electron., vol. 3, no. 5, pp. 267–272, May 2020.

[6] H. Yao et al., "Twist piezoelectricity: giant electromechanical coupling in magic-angle twisted bilayer LiNbO3," Nat. Commun., vol. 15, no. 1, p. 5002, Jun. 2024.

[7] Y. Yang, R. Lu, L. Gao, and S. Gong, "4.5 GHz Lithium Niobate MEMS Filters With 10% Fractional Bandwidth for 5G Front-Ends," J. Microelectromechanical Syst., vol. 28, no. 4, pp. 575–577, Aug. 2019.

[8] Y. Yang, R. Lu, L. Gao, and S. Gong, "10–60-GHz Electromechanical Resonators Using Thin-Film Lithium Niobate," IEEE Trans. Microw. Theory Tech., vol. 68, no. 12, pp. 5211–5220, Dec. 2020.

[9] J. Wang, M. Park, S. Mertin, T. Pensala, F. Ayazi, and A. Ansari, "A Film Bulk Acoustic Resonator Based on Ferroelectric Aluminum Scandium Nitride Films," J. Microelectromechanical Syst., vol. 29, no. 5, pp. 741–747, Oct. 2020.

[10] C. Cassella and J. Segovia-Fernandez, "High kt2 Exceeding 6.4% Through Metal Frames in Aluminum Nitride 2-D Mode Resonators," IEEE Trans. Ultrason. Ferroelectr. Freq. Control, vol. 66, no. 5, pp. 958–964, May 2019.

[11] R. Vetury, M. D. Hodge, and J. B. Shealy, "High Power, Wideband Single Crystal XBAW Technology for sub-6 GHz Micro RF Filter Applications," in 2018 IEEE International Ultrasonics Symposium (IUS), Kobe: IEEE, Oct. 2018, pp. 206–212.

[12] T. Takai et al., "High-Performance SAW Resonator on New Multilayered Substrate Using LiTaO3 Crystal," IEEE Trans. Ultrason. Ferroelectr. Freq. Control, vol. 64, no. 9, pp. 1382–1389, Sep. 2017.

[13] Z. Schaffer, A. Hassanien, M. A. Masud, and G. Piazza, "A Solidly Mounted 55 GHz Overmoded Bulk Acoustic Resonator," in 2023 IEEE International Ultrasonics Symposium (IUS), Montreal, QC, Canada: IEEE, Sep. 2023, pp. 1–4.

[14] O. Barrera et al., "Thin-Film Lithium Niobate Acoustic Filter at 23.5 GHz With 2.38 dB IL and 18.2% FBW," J. Microelectromechanical Syst., vol. 32, no. 6, pp. 622–625, Dec. 2023.

[15] L. Shao et al., "Electrical control of surface acoustic waves," Nat. Electron., vol. 5, no. 6, pp. 348–355, Jun. 2022.

[16] S. Shao, Z. Luo, and T. Wu, "Electro-Acoustic Phase Modulator Based on AlScN Thin Film," IEEE Electron Device Lett., vol. 44, no. 5, pp. 817–820, May 2023.

[17] L. Shao, S. W. Ding, Y. Ma, Y. Zhang, N. Sinclair, and M. Lončar, "Thermal Modulation of Gigahertz Surface Acoustic Waves on Lithium Niobate," Phys. Rev. Appl., vol. 18, no. 5, p. 054078, Nov. 2022.

[18] J. C. Taylor, E. Chatterjee, W. F. Kindel, D. Soh, and M. Eichenfield, "Reconfigurable quantum phononic circuits via piezo-acoustomechanical interactions," Npj Quantum Inf., vol. 8, no. 1, p. 19, Feb. 2022.

[19] M. Yamagata, N. Cao, D. D. John, and H. Hashemi, "Surface-Acoustic-Wave Waveguides for Radio Frequency Signal Processing," IEEE Trans. Microw. Theory Tech., vol. 71, no. 3, pp. 931–944, Mar. 2023.

[20] R. Lu, Y. Yang, S. Link, and S. Gong, "A1 Resonators in 128° Y-cut Lithium Niobate with Electromechanical Coupling of 46.4%," J. Microelectromechanical Syst., vol. 29, no. 3, pp. 313–319, Jun. 2020.

[21] R. Lu, Y. Yang, S. Link, and S. Gong, "Low-Loss 5-GHz First-Order Antisymmetric Mode Acoustic Delay Lines in Thin-Film Lithium Niobate," IEEE Trans. Microw. Theory Tech., vol. 69, no. 1, pp. 541–550, Jan. 2021.

[22] Y. Yang, R. Lu, and S. Gong, "High Q Antisymmetric Mode Lithium Niobate MEMS Resonators with Spurious Mitigation," J. Microelectromechanical Syst., vol. 29, no. 2, pp. 135–143, Apr. 2020.

[23] K. Liu, Y. Lu, and T. Wu, "7.5 GHz Near-Zero Temperature Coefficient of Frequency Lithium Niobate Resonator," IEEE Electron Device Lett., vol. 44, no. 2, pp. 305–308, Feb. 2023.

[24] J. W. Stewart, J. H. Vella, W. Li, S. Fan, and M. H. Mikkelsen, "Ultrafast pyroelectric photodetection with on-chip spectral filters," Nat. Mater., vol. 19, no. 2, pp. 158–162, Feb. 2020.

[25] L. Wei, Z. You, X. Kuai, M. Zhang, F. Yang, and X. Wang, "MEMS thermal-piezoresistive resonators, thermal-piezoresistive oscillators, and sensors," Microsyst. Technol., vol. 29, no. 1, pp. 1–17, Jan. 2023.

[26] W. Xu, X. Wang, Z. Ke, and Y.-K. Lee, "Bidirectional CMOS-MEMS Airflow Sensor with Sub-mW Power Consumption and High Sensitivity," IEEE Trans. Ind. Electron., vol. 69, no. 3, pp. 3183–3192, Mar. 2022.

[27] X. Chen et al., "Fast-Response Thin Film Heat Flux Sensors for Harsh Environments," IEEE Sens. J., vol. 24, no. 12, pp. 18844–18850, Jun. 2024.

[28] M. H. Li, C. Y. Chen, R. Lu, Y. Yang, T. Wu, and S. Gong, "Temperature Stability Analysis of Thin-Film Lithium Niobate SH0 Plate Wave Resonators," J. Microelectromechanical Syst., vol. 28, no. 5, pp. 799–809, Oct. 2019.